Journal of Molecular Structure 1140 (2017) 2–11

Contents lists available at ScienceDirect

Journal of Molecular Structure

journal homepage: http://www.elsevier.com/locate/molstruc

Analysis of the structure and the FT-IR and Raman spectra of 2-(4-nitrophenyl)-4H-3,1-benzoxazin-4-one. Comparisons with the chlorinated and methylated derivatives

María V. Castillo [a], Roxana A. Rudyk [a], Lilian Davies [b], Silvia Antonia Brandán [a, *]

[a] Cátedra de Química General, Instituto de Química Inorgánica, Facultad de Bioquímica, Química y Farmacia, Universidad Nacional de Tucumán, Ayacucho 471, 4000, San Miguel de Tucumán, Tucumán, R, Argentina
[b] Instituto de Investigaciones para la Industria Química (INIQUI, CONICET), Universidad Nacional de Salta, Av. Bolivia 5150, 4400, Salta, Argentina

ARTICLE INFO

Article history:
Received 8 June 2016
Received in revised form
22 August 2016
Accepted 25 August 2016
Available online 26 August 2016

Keywords:
Benzoxazin derivatives
Vibrational spectra
Molecular structure
Force field
DFT calculations

ABSTRACT

In this work, the structural, topological and vibrational properties of the monomer and three dimers of the 2-(4-nitrophenyl)-4H-3,1-benzoxazin-4-one (NPB) derivative were studied combining the experimental FTIR and FT-Raman spectra in the solid phase with DFT calculations. Here, Natural Bond Orbital (NBO), Atoms in Molecules (AIM) and HOMO and LUMO calculations were performed by using the hybrid B3LYP/6-31G*and B3LYP/6-311++G** methods in order to compute those properties and to predict their reactivities. The comparisons with the properties reported for the chlorinated (Cl-PB) and methylated (CH_3-PB) derivatives at the same levels of theory can be clearly justified by the activating (CH_3) and deactivating (NO_2 and Cl) characteristics of the different groups linked to oxaxin rings. The NBO and AIM studies evidence the following stability orders: Cl-PB > NO_2-PB > CH_3-PB in very good concordance with the *f(νC23-X26)* force constants values. The frontier orbitals analyses reveal that the Cl-PB and NO_2-PB derivatives have good stabilities and high chemical hardness while CH_3-PB has a higher chemical reactivity. On the other hand, the complete vibrational assignments for monomer and dimers species of NPB were presented. The presence of the IR bands at 1574 and 1037 cm^{-1} and, of the Raman bands at 1571 and 1038 cm^{-1} support clearly the presence of the different dimeric species proposed for NPB.

1. Introduction

As part of our investigations on heterocyclic derivatives containing different rings such as, isothiazoles, benzothiazole, oxadiazole, quinolin [1–5], in the present work, we have reported the structural and vibrational studies of the 2-(4-nitrophenyl)-4H-3,1-benzoxazin-4-one derivative by using their experimental infrared and Raman spectra in the solid phase and DFT calculations. Some 4*H*-3,1-benzoxazin-4-ones derivatives present a wide range of potential biological activities such as, antitumor, antimicrobial, antitubercular, antimalaria, anticonvulsant, anthelmintic, anti-inflammatory and analgesic among others [6–8]. Industrially, these derivatives are used in the preparation of soluble and processable polybenzoxazine precursors capable of forming high performance networks, as reported by Altinkok et al. [9] while, in chemical synthesis these derivatives are also used to obtain novel quinazolinone derivatives of pharmacological interest [10,11]. Structurally, the 4*H*-3,1-benzoxazin-4-one derivatives have a benzene ring fused to an oxazin ring and with the incorporation of different groups in some of these rings or, in both, their chemical and pharmacological properties are modified. The 2-(4-nitrophenyl)-4H-3,1-benzoxazin-4-one (NPB) derivative was synthesized and characterized by Rai [12] by using the NMR and infrared spectra but, so far, its experimental structure was not reported and neither their Raman spectrum and only few IR bands were assigned. In this context, the aims of this work are: (i) to study the theoretical structures of NPB in gas phase by using the hybrid B3LYP method and the 6-31G* and 6-311++G** basis sets, (ii) to evaluate the atomic charges, molecular electrostatic potentials, bond orders, stabilization energies and the topological properties using both theory levels, (iii) to perform the vibrational analyses by using the IR and Raman spectra and compute the corresponding force fields in order to assign all the observed bands in those spectra, (iv) to predict the reactivities and behaviors by using the

* Corresponding author.
E-mail address: sbrandan@fbqf.unt.edu.ar (S.A. Brandán).

http://dx.doi.org/10.1016/j.molstruc.2016.08.070
0022-2860/

frontier orbitals and some reported descriptors at the same level of calculations and, finally, (v) to analyze the changes in all the properties when activating (CH_3) and deactivating groups (NO_2 and Cl) are incorporated to the benzene ring linked to the 4H-3,1-benzoxazin-4-one ring. In this way, the properties of NPB are compared with those reported for 2-(4-chlorophenyl)-4H-3,1-benzoxazin-4-one (CPB) and 2-(4-methylphenyl)-4H-3,1-benzoxazin-4-one (MPB) [13,14]. In this study, the presence of dimeric species of NPB were also considered because these species justify some bands observed in the vibrational spectra. This way, NPB could be easily identified by means of the vibrational spectroscopy and, in addition, this work constitutes a very important database to understand the connection that exists between the different groups present in the structure of a 4H-3,1-benzoxazin-4-one derivative in relation to their biological properties.

2. Experimental methods

The solid anhydrous commercial sample of 2-(4-nitrophenyl)-4H-3,1-benzoxazin-4-one in pure form was used to prepare KBr pellets. The infrared spectrum was recorded on a Fourier Transform Infrared (FT-IR) Perkin Elmer spectrophotometer in the wavenumbers range from 4000 to 400 cm^{-1} provided with a Globar source and DGTS detector. The Raman spectra of the compound in solid state was recorded between 4000 and 10 cm^{-1} with a Bruker RF100/S spectrometer equipped with a Nd:YAG laser (excitation line of 1064 nm, 800 mW of laser power) and a Ge detector cooled at liquid nitrogen temperature. The IR and Raman spectra were recorded with 200 scans and a resolution of 1 cm^{-1}.

3. Computational details

Initially, the monomeric NPB structure was modeled with the *GaussView* program [15], after that, the hybrid B3LYP method [16,17] and the 6-31G* and 6-311++G** basis sets were used to optimize both structures with the Gaussian 09 program [18]. The theoretical monomeric structure can be seen in Fig. 1 together with the atoms numbering and identifications of the three six-membered rings. Hence, A1 is the phenyl ring fused with the oxazin ring which is identified as A2 while A3 is the phenyl ring containing the NO_2 group. Then, three different dimeric species of NPB were also optimized by using the B3LYP/6-31G* method and, their structures are given in Fig. S1. The calculations of the atomic natural population (NPA) charges, bond orders and stabilization energies were computed by using the NBO program [19,20] while the molecular electrostatic potentials (MEP) were calculated from the Merz-Kollman charges [21]. The topological properties of the three rings of NPB were computed by using the atoms in molecules (AIM) calculations in accordance with the Bader's theory [22,23]. The harmonic frequencies were calculated from the optimized structures by using both approximation levels while the normal internal coordinates for NPB were defined in accordance to those reported for the CPB and MPB derivatives [13,14] and, for this reason, these coordinates for NPB were not presented here. The force fields were calculated by means of the Molvib program by using both basis sets [24] and the scaled quantum mechanical (SQM) methodology [25]. On the other hand, the reactivities and behaviors of NPB with the different basis sets were predicted by using the frontier orbitals, computing the energy band gap and some practical descriptors such as, chemical potential (μ), electronegativity (χ), global hardness (η), global softness (S) and global electrophilicity index (ω). The equations corresponding to these descriptors are widely known in the literature [1,2,26] and, therefore, they were presented in the Supporting material together with the calculated values for NPB with both basis sets and with those reported for the CPB and MPB derivatives [13,14].

4. Results and discussion

4.1. Geometry optimizations

A comparison of the dipole moment values for the two stable structures of NPB with those corresponding to CPB [13] and MPB [14] by using both methods are shown in Table 1. As it was expected, both methods predicted energy values in the following order: CPB > NPB > MPB. On the other hand, the dipole moment values present different values and directions according to the activating and deactivating characteristics of each group

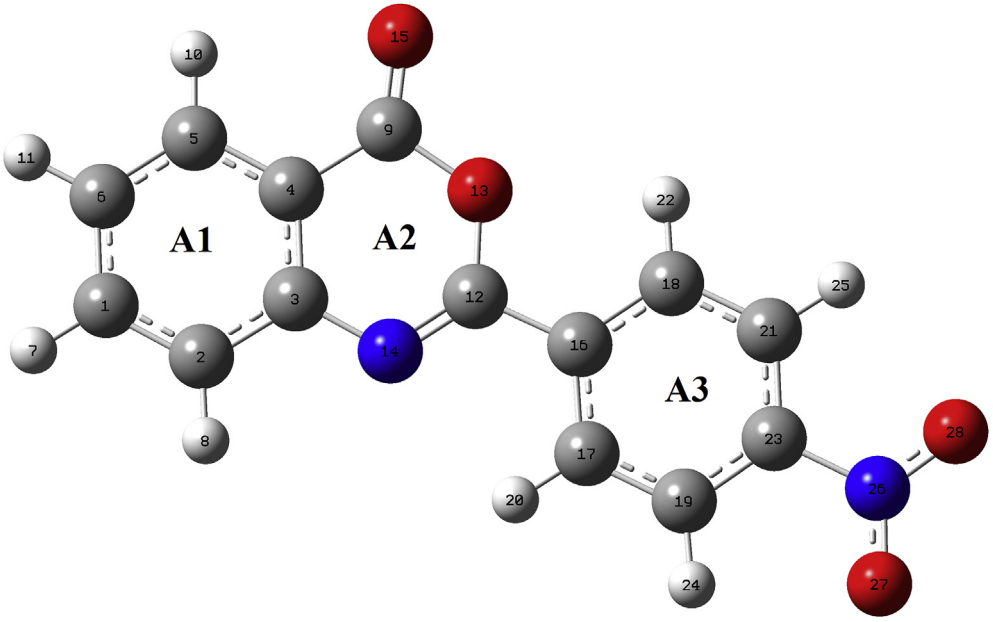

Fig. 1. Theoretical structure and atoms numbering of 2-(4-nitrophenyl)-4H-3,1-benzoxazin-4-one.

Table 1
Calculated total energy (E) and dipolar moments for 2-(4-nitrophenyl)-4H-3,1-benzoxazin-4-one compared with 2-(4-chlorophenyl)-4H-3,1-benzoxazin-4-one and 2-(4-methylphenyl)-4H-3,1-benzoxazin-4-one derivatives at different levels of theory.

B3LYP method		
2-(4-nitrophenyl)-4H-3,1-benzoxazin-4-one[a]		
Property	6-31G*	6-311++G**
E (Hartrees)	−948.6371	−948.8899
μ (D)	5.81	6.29
2-(4-chlorophenyl)-4H-3,1-benzoxazin-4-one[b]		
E (Hartrees)	−1203.7336	−1203.9517
μ (D)	3.10	3.30
2-(4-methylphenyl)-4H-3,1-benzoxazin-4-one[c]		
E (Hartrees)	−783.4568	−783.6576
μ (D)	3.01	3.26

[a] This work.
[b] From Ref. [13].
[c] From Ref. [14].

incorporated to the A3 ring, being the CH_3 group an activating agent while the Cl atom and NO_2 group act as deactivating. Thus, the values decrease according to the following order: $NO_2 > Cl > CH_3$, hence, the tendency is: NPB > CPB > MPB. This way, the dipole moments are oriented toward the benzoxazin ring in NPB and CPB due to the presence of the respective deactivating NO_2 and Cl groups, as observed in Fig. 2 while, on the contrary, in MPB due to the presence of an activating CH_3 group the dipole moment is oriented towards the methyl-phenyl ring. Note that the energy and dipole moment values are strongly dependent on the method used, as can be seen in Table 1. Thus, both properties are enlarged when the size basis set increase from 6-31G* to 6-311++G**.

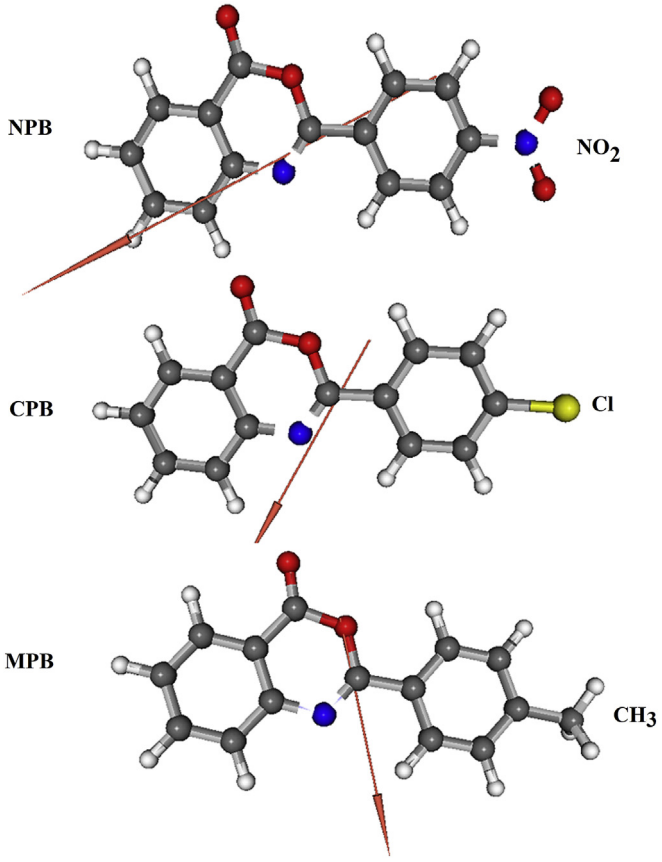

Fig. 2. Calculated magnitude and orientation of the dipole moments for 2-(4-nitrophenyl)-4H-3,1-benzoxazin-4-one (NPB), 2-(4-chlorophenyl)-4H-3,1-benzoxazin-4-one (CPB) and 2-(4-methylphenyl)-4H-3,1-benzoxazin-4-one (MPB) by using the B3LYP/6-311++G** method indicating the different groups present in each derivative.

So far, the NPB structure was not experimentally determined, for this reason, the geometrical parameters calculated by using both methods were compared with those experimental determined for 2-phenyl-4*H*-3,1-benzoxazin-4-one (PB) by X-ray diffraction by Thilagavathy et al. [27] in Table 2. In that experimental PB structure the dihedral angle between the plane of the phenyl ring and the 3,1-benzoxazin-4-one fragment is of 3.7° (4). On the contrary, the theoretical calculations predict the structure of NPB as essentially planar with torsion angles of 180 or 0°, as can be seen in Table 2. The comparisons performed by means of the root means of square deviations (rmsd) values show very good concordance with both basis sets in the bond lengths (0.003 Å) and in the bond angles (0.11°). Here, the calculated C12—N14 distances by using both calculation levels are predicted with a certain double bond character, as it was also experimentally observed in CPB [13]. We think that probably, the molecular structure of NPB is also stabilized by intermolecular C—H—O hydrogen bonds as in PB, whose crystal packing are stabilized by weak intermolecular C—H—O and π-π stacking interactions [27,28] and, for this reason, three different dimeric species were considered.

4.2. Molecular electrostatic potentials, NPA charges and bond orders

Taking into account the potential biological properties of NPB, the molecular electrostatic potentials (MEPs) and the NPA charges were studied by using both levels of theory in order to investigate the electrophilic and nucleophilic sites. Thus, the results for both basis set are summarized in Table S1 together with the bond order values. Analyzing first the NPA charges, the most negative values are observed on the two O13 and O15 atoms of the oxaxin ring which present the higher values than the other ones while on the N14 atoms of that ring are observed the most negative values. Thus, on the N26 atoms positive charges are observed, as it was expected because these atoms belong to the NO_2 groups where both atoms are linked to the O atoms with negative charges. Here, the effect of increment of the size of the basis set is observed in the diminishing of the charge values. Note that on the H24 and H25 atoms nearer to the NO_2 groups the most positive charge values are observed and, they are higher than the other ones.

In relation to the MEP values, Table S1 shows that the highest negative values are observed on all the O atoms where, in particular, the O13 atoms belong to the oxaxin ring have the least values while the N26 atoms belong to the NO_2 groups present the lowest values in relation to the N14 atoms of the oxaxin ring which show the most negative values. On the other hand, analyzing the values for the H atoms it is observed that the H24 and H25 atoms present the least negative values; hence, these results are in agreement with the NPA values. The different charges and MEP values observed on the atoms of NPB can be easily evidenced by their different colorations in the MEP surface mapped. Thus, Fig. S2 shows the MEP surface mapped for NPB using the 6-31G* basis set. Here, the nucleophilic sites are clearly observed in red colour on all the O atoms while the electrophilic sites are observed on the H atoms. Notice that the O15 atom presents a strong red colour in accordance to the highest charge and MEP values, as indicated in Table S1.

In relation to the bond order values expressed as Wiberg indexes, and presented in Table S1 the analysis shows that the highest values are observed in the C3 and C4 atoms which are common atoms to the oxaxin rings and, in the C16 and C23 atoms of the A3

Table 2
Calculated geometrical parameters for the 2-(4-nitrophenyl)-4H-3,1-benzoxacin-4-one compared with the experimental values for 2-phenyl-4*H*-3,1-benzoxazin-4-one.

Parameter	B3LYP method[a]		Experimental[b]
	6-31G*	6-311++G**	
Bond length (Å)			
C1–C2	1.389	1.386	1.369 (2)
C2–C3	1.405	1.403	1.394 (2)
C3–C4	1.413	1.411	1.393 (2)
C4–C5	1.402	1.401	1.387 (2)
C5–C6	1.388	1.386	1.371 (2)
C4–C9	1.462	1.461	1.448 (2)
C1–C6	1.405	1.403	1.381 (3)
C9–O15	1.204	1.197	1.193 (19)
C9–O13	1.406	1.406	1.379 (19)
C12–O13	1.366	1.364	1.370 (18)
C12–N14	1.286	1.281	1.275 (2)
C12–C16	1.476	1.476	1.462 (2)
C3–N14	1.388	1.388	1.394 (2)
C16–C17	1.406	1.403	1.384 (2)
C16–C18	1.404	1.402	1.388 (2)
C17–C19	1.388	1.386	1.371 (2)
C18–C21	1.391	1.389	1.376 (3)
C19–C23	1.395	1.393	1.374 (3)
C21–C23	1.393	1.390	1.391 (16)
C23–N26	1.473	1.481	1.478 (11)
N26–O27	1.230	1.224	1.226
N26–O28	1.230	1.224	1.218
RMSD	**0.003**	**0.003**	
Bond angle (degrees)			
C1–C2–C3	119.9	119.9	119.5 (16)
C2–C3–C4	119.1	119.1	119.1 (15)
C3–C4–C5	120.6	120.6	120.6 (15)
C4–C5–C6	119.6	119.7	119.6 (16)
C5–C6–C1	120.0	120.0	120.0 (17)
C2–C1–C6	120.8	120.8	121.3 (16)
C3–C4–C9	119.0	119.0	118.7 (15)
C5–C4–C9	120.3	120.4	120.7 (15)
C12–C16–C17	119.1	119.2	119.2 (15)
C17–C16–C18	119.8	119.8	119.3(17)
O13–C9–C4	114.2	114.1	115.3 (14)
O15–C9–C4	128.0	128.2	127.7 (16)
C16–C17–C19	120.3	120.4	120.2 (18)
C12–C16–C18	121.1	121.0	121.7(16)
C17–C19–C23	118.7	118.7	119.9 (2)
C19–C23–C21	122.1	122.1	120.6 (19)
C21–C23–N26	118.9	118.9	119.7
C19–C23–N26	118.9	118.9	119.7
C18–C21–C23	118.8	118.8	119.9 (2)
C12–O13–C9	122.0	122.1	121.6 (12)
N14–C12–O13	125.1	125.0	124.7 (15)
N14–C12–C16	122.0	122.2	122.9 (15)
C3–N14–C12	118.0	118.1	117.8 (14)
C2–C3–N14	119.2	119.2	119.2 (15)
C4–C3–N14	121.7	121.7	121.7 (14)
O13–C12–C16	112.9	112.9	112.4 (14)
O15–C9–O13	117.7	117.7	117.0 (15)
C16–C18–C21	120.2	120.2	120.0 (19)
C23–N26–O27	117.6	117.6	117.4 (10)
C23–N26–O28	117.6	117.6	118.2 (10)
O27–N26–O28	124.8	124.8	124.4 (10)
RMSD	**0.11**	**0.11**	
Dihedral angles (degrees)			
C19–C17–C16–C18	0.0	0.0	0.9 (2)
C17–C16–C18–C21	0.0	0.0	−0.4 (3)
C16–C18–C21–C23	0.0	0.0	0.0 (3)
C18–C21–C23–C19	0.0	0.0	−0.1 (3)
C21–C23–C19–C17	0.0	0.0	0.7 (3)
C23–C19–C17–C16	0.0	0.0	−1.0 (3)
C19–C17–C16–C12	180.0	180.0	−179.3 (15)
C2–C3–C4–C9	180.0	−180.0	178.2 (14)
C2–C3–C4–C5	0.0	0.0	−0.8 (2)
N14–C3–C4–C5	−180.0	180.0	178.7 (14)
C6–C1–C2–C3	0.0	0.0	−0.3 (3)
N14–C3–C4–C9	0.0	0.0	−2.3 (2)
C5–C6–C1–C2	0.0	0.0	−0.6 (3)
C4–C5–C6–C1	0.0	0.0	0.8 (3)
N14–C12–O13–C9	0.0	0.0	0.1 (2)
C2–C3–N14–C12	180.0	−180.0	179.8 (15)
C4–C3–N14–C12	0.0	0.0	0.2 (2)
C3–N14–C12–C16	180.0	180.0	−179.6 (12)
C3–N14–C12–O13	0.0	0.0	0.9 (2)
C1–C2–C3–N14	180.0	180.0	−178.6 (14)
C1–C2–C3–C4	0.0	0.0	1.0 (2)
N14–C12–C16–C17	0.0	0.0	−3.3 (2)
C5–C4–C9–O13	−180.0	180.0	−177.9 (14)
C5–C4–C9–O15	0.0	0.0	3.1 (3)
O13–C12–C16–C18	0.0	0.0	−3.7 (4)
O13–C12–C16–C17	−180.0	180.0	176.3 (13)
C14–C12–C16–C18	−180.0	−180.0	176.5 (15)
C12–C16–C18–C21	180.0	180.0	179.9 (15)
C9–O13–C12–C16	−180.0	180.0	−179.4 (13)
C3–C4–C9–O15	−180.0	180.0	−175.8 (17)
O15–C9–O13–C12	180.0	−180.0	176.9 (16)
C3–C4–C9–O13	0.0	0.0	3.1 (2)
C4–C9–O13–C12	0.0	0.0	−2.1 (2)
C3–C4–C5–C6	0.0	0.0	−0.1 (2)
C9–C4–C5–C6	180.0	−180.0	−179.0 (15)
C17–C19–C23–N26	180.0	180.0	179.6 (10)
C18–C21–C23–N26	180.0	180.0	−180.0 (10)
C21–C23–N26–O27	−180.0	−180.0	167.2 (11)
C21–C23–N26–O28	0.0	0.0	- 12.7(16)
C19–C23–N26–O27	0.0	0.0	−12.2 (16)
C19–C23–N26–O28	−180.0	−180.0	167.9 (11)
RMSD	**27.5**	**31.4**	

[a] This work.
[b] From Ref. [27].

ring. On the other hand, both O atoms belong to the NO_2 group present double bond character, as shown in Fig. 1. Analyzing the values for the H atoms, the most labile H atoms are observed in the two H24 and H25 atom which present lower charge and MEP values.

4.3. NBO and AIM studies

The stabilities for NPB with both basis sets were also studied in gas phase by using NBO and AIM calculations. Thus, in Table S2 the donor-acceptor interaction energies obtained from the second order perturbation calculations for NPB are reported with both basis sets. Here, only those interactions between different rings and rings and substituent's were considered in this study. The results show a high stability in that medium with both basis sets which are strongly related to the $\Delta ET_{\sigma \rightarrow \sigma^*}$, $\Delta ET_{\sigma^* \rightarrow \sigma^*}$ and $\Delta ET_{n \rightarrow \sigma^*}$ charge transfers due to the C=C and C=O of the different rings and to the lone pairs of the N14 atoms and of the four O atoms. Besides, additional *σC21-C23 → LP(3)O27* transitions of low energies that slightly stabilize the A3 rings are observed with both basis sets. The highest contributions to the ΔE_{Total} values are observed in the $\Delta ET_{\sigma^* \rightarrow \sigma^*}$ charge transfers from different anti-bonding orbitals towards other anti-bonding orbitals that belong to the A2 and A3 rings. Note that when the size of the basis set increase to 6-311++G** some transitions decrease their values ($\Delta ET_{\sigma \rightarrow \sigma^*}$ and $\Delta ET_{n \rightarrow \sigma^*}$) whiles other increase ($\Delta ET_{\sigma^* \rightarrow \sigma^*}$) and, as a consequence the ΔE_{Total} values are also increased. When the total stabilization energy value of NPB (5803.1 kJ/mol) using the 6-31G* basis set is compared with those reported for CPB (6804.41 kJ/mol) [13] and MPB (3992.23 kJ/mol) [14] at the same level of theory we observed that effectively the activating agent (CH_3 group) decreases the

stability of the A3 ring and as a consequence it makes A3 more reactive because it donates electrons to the benzoxazin-4-one ring while the substituent deactivating (Cl atom and NO_2 group) makes less reactive withdraw electrons from the benzoxazin-4-one ring stabilizing the compound ($>\Delta E_{Total}$). Here, the stability orders with both basis sets are: CPB > NPB > MPB.

We also have investigated the stability of NPB by using of Bader's theory by means of calculations of the topological properties with the AIM2000 program [22,23]. Thus, the calculated charge electron density, *(ρ)* and the *Laplacian* values, $\nabla^2\rho(r)$ in the ring critical points (RCPs) of A1, A2 and A3 rings with both level of theory are shown in Table S3 compared with those reported for CPB and MPB and, also with those calculated in this work, for the PB derivative. Here, RCP_1 corresponds to the phenyl ring fused with the oxazin moiety, RCP_2 corresponds to the oxazin ring while the RCP_3 corresponds to the nitrophenyl, chlorophenyl, methyl or phenyl ring, in accordance with NPB, MPB, CPB or PB, respectively. The analysis clearly shows that the three RCPs have different topological properties having A3 the highest values in the fours derivatives and, the values for A1 and A2 remain practically constant when the basis set increases from 6-31G* to 6-311++G**. Also, the density values increase with the basis set while the *Laplacian* values, in general,-decrease. The inspection exhaustive reveals that using the 6-311++G** basis set those two properties decrease according the following order: PB > NPB > CPB > MPB. The lowest density values for MPB confirm that the activating CH_3 group decrease the stability of the A3 ring and as a consequence make A3 more reactive while the values are slightly higher for NPB and CPB (NO_2 group and Cl atom) than MPB, deactivating the benzoxazin-4-one ring stabilizing the compound. These results are in very good agreement with those obtained by NBO analysis.

4.4. Frontier HOMO-LUMO

The frontier orbitals are useful to analyze the reactivity of different species by using the energy gap values calculated as the difference observed between the HOMO and LUMO, thus, a species is more reactive than other when the gap value is lower [26]. Moreover, it is possible to predict the behaviour of diverse systems using the chemical potential (μ), electronegativity (χ), global hardness (η), global softness (S) and global electrophilicity index (ω) descriptors calculated with those two orbitals by means of equations reported in the literature and presented in Table S4 [29–33]. The results for NPB by using both basis sets are compared in Table S4 with those reported for PB, CPB and MPB [13,14] at the same level of theory. These properties show clearly that the reactivity increases showing the following order: MPB < CPB < PB < NPB. Moreover, the results show that when the Cl atom or the NO_2 group is incorporated to the benzoxazin-4-one ring in PB clearly increases the reactivity because both species deactivates that ring. However, when the group incorporated is the activating CH_3 group, it reactives the benzoxazin-4-one ring but in this case MPB is less reactive than PB. Evidently, there is another more important factor different from the gap value that has influence on the reactivity. Thus, analyzing the HOMO values the reactivity increases according to the following order: NPB > CPB > PB > MPB, which are in complete concordance with the highest reactivity for MPB because, it has an activating grouping that makes the benzoxazin-4-one ring more reactive. On the contrary, the deactivating NO_2 group decreases the reactivity of that ring and, as a consequence the reactivity of NPB. Those gap values indicating that NPB and CPB have good stabilities and high chemical hardness while PB and MPB have a higher chemical reactivity. Thus, the introduction of a Cl atom or a NO_2 group in the benzoxazin ring increases the stability of the corresponding derivative. On the other hand, analyzing the descriptors for all the species, we observed that the activating CH_3 group decreases the electrophilicity index of PB, as compared with MPB while the presence of deactivating NO_2 group increases that index. This way, the electrophilicity index is higher in NPB as compared with PB.

4.5. Vibrational study

The optimized NPB structure has C_1 symmetry and 78 normal vibration modes where all these modes are active in the infrared and Raman spectra. The FTIR and FT-Raman spectra in the solid phase for the monomer are observed in Figs. 3 and 4 compared with the corresponding predicted for this species by using the B3LYP/6-31G* method and, with the predicted for the three different dimeric

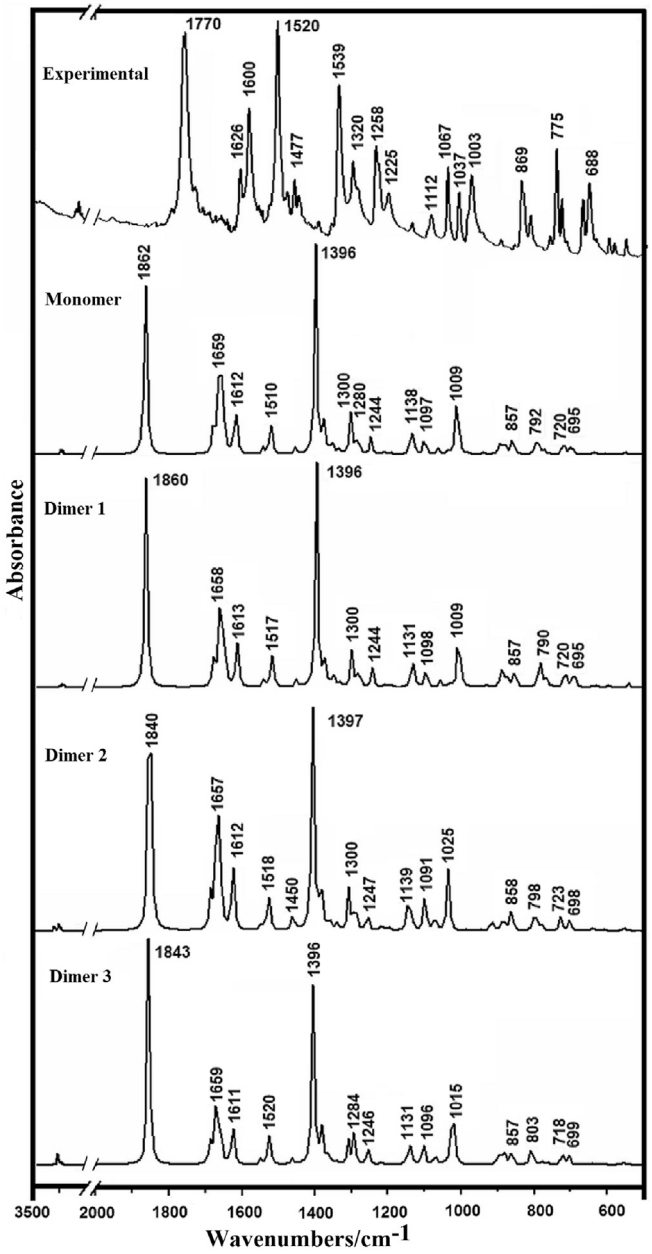

Fig. 3. Experimental infrared spectra of 2-(4-nitrophenyl)-4H-3,1-benzoxazin-4-one in solid phase compared with the corresponding predicted for the monomer and three dimeric species by using the B3LYP/6-31G* method.

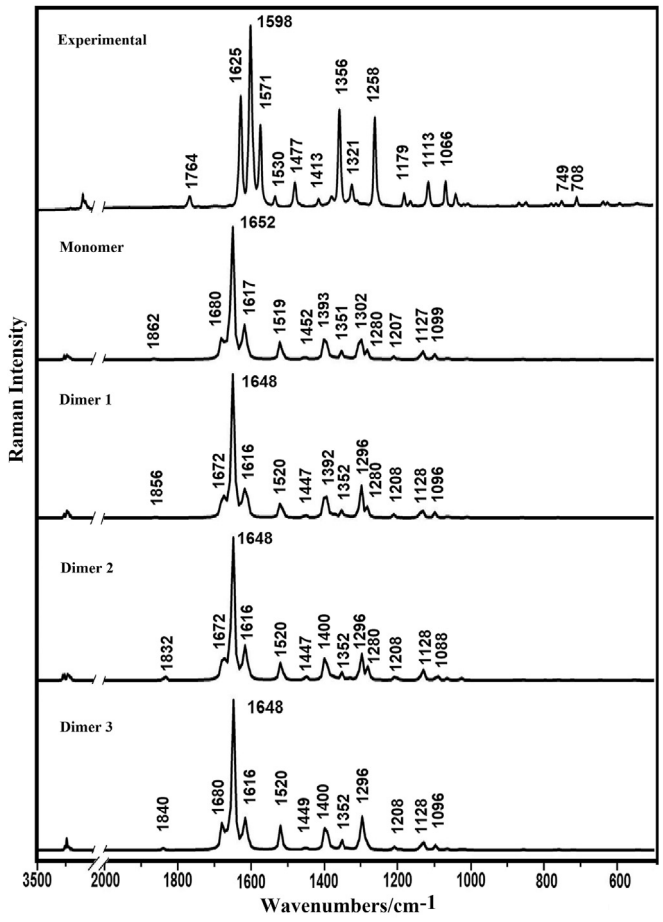

Fig. 4. Experimental Raman spectra of 2-(4-nitrophenyl)-4H-3,1-benzoxazin-4-one in solid phase compared with the corresponding predicted for the monomer and three dimeric species by using the B3LYP/6-31G* method.

species in accordance with the experimental structure reported for 2-phenyl-4*H*-3,1-benzoxazin-4-one (PB) by Thilagavathy et al. [27]. Here, the presence of three different dimeric species could probably explain some bands observed in both spectra which are not assigned to the monomer. The experimental and calculated wavenumbers for the expected normal vibration modes of NPB, the SQM/B3LYP/6-31G* calculations, and the corresponding assignments are shown in Table 3. The calculated and observed wavenumbers, potential energy distribution and assignment for NPB are given in Table S5. Fig. S3 shows a comparison between the infrared experimental spectrum of NPB in solid phase with the calculated infrared spectra for the monomer and three dimeric species from B3LYP/6-31G* frequencies and intensities using Lorentzian band shapes (for a population relation *dimer1: dimer2: dimer3* of 1: 1: 1 for each species). This way, the average spectrum of the three dimeric species, taking into account the populations (1: 1: 1 ratio) reproduce rather well some bands of the experimental spectrum, as indicated in circle in Fig. S3. Here, it is very important to clarify that the assignments of the three dimeric species were performed with the aid of the *GaussView* program [15]. At this point, the group of the observed weak IR bands in the 3053-2872 cm^{-1} region could probably be attributed to combinations bands or to the hydrogen bonds as a consequence of crystal packing of NPB, as also was reported for CPB [27], as suggested in Table 3. In this study, the vibrational assignment of the experimental bands to the normal vibration modes was performed taking into account the assignments reported for similar molecules [13,14] and the calculation's results performed in this study. In this case, we have considered the B3LYP/6-31G* calculations in accordance to the used scale factors for this calculation level. The calculated SQM force field for NPB can be obtained at the request of the authors. Below, a brief discussion of the assignments of some important groups is presented.

4.5.1. Bands assignments

4.5.1.1. CH modes. For NPB eight C—H stretching modes are expected, four belonging to the A1 ring and four to the A3 ring. These modes are clearly predicted by SQM calculations in the 3122-3065 cm^{-1} region, as reported in similar compounds [13,14,30–33]. Note that the C—H stretching modes for A3 are predicted at higher wave numbers than A1 due to the presence of the NO_2 group in A3. Hence, those modes are assigned to the IR bands between 3192 and 3082 cm^{-1} region and to the Raman bands observed between 3194 and 3063 cm^{-1}, as observed in Table 3. Obviously, eight in-plane and out-of-plane deformation modes are also expected for NPB. Thus, for the monomer those modes are predicted at 1492/1105 and 998/785 cm^{-1} while in the dimeric species those modes are predicted at 1539/1034 and 1025/718 cm^{-1}, respectively.

4.5.1.2. NO_2 modes. Here, two NO_2 antisymmetrical and symmetric stretching modes are expected for the monomer of NPB while for the dimeric species four stretching modes. In the thiol and thione forms of 1,3-benzothiazole tautomers, the antisymmetrical stretching modes are assigned at 1584 and 1540 cm^{-1}, respectively while the corresponding symmetric modes for both forms were assigned at 1335 cm^{-1} [32]. Here, the strong IR bands at 1520 and 1359 cm^{-1} can easily be attributed to those modes for the monomeric species of NPB while the strong Raman band at 1571 cm^{-1} can be assigned to the in-phase antisymmetrical stretching modes of the dimeric species. This way, the presence of the infrared and Raman bands at 1574 and 1571 cm^{-1}, respectively justify clearly the presence of those three dimeric species of NPB. In the two 1,3-benzothiazole tautomers [32] the NO_2 deformation modes of thione and thiol, respectively are assigned at 841 and 821 cm^{-1} while the wagging modes of both forms are assigned to the IR band at 756 cm^{-1}. In monomer and dimers of NPB, the NO_2 deformation and wagging modes are predicted in the same region, hence, they were assigned to the weak band at 845 cm^{-1} and to the strong band at 775 cm^{-1}, respectively. Also, the rocking modes of monomer and dimers are clearly predicted in the same region and, for this reason, those modes are assigned to the weak IR band at 532 cm^{-1}, in accordance to those two tautomers which were assigned at 545 cm^{-1} [32]. The twisting modes for the monomer and dimers are predicted by SQM calculations between 66 and 63 cm^{-1} while in those two thiol and thione tautomers these modes are predicted at 51 and 52 cm^{-1}, respectively [32]. Due to the low wavenumbers values these modes could not be assigned. This study shows clearly that all the vibration modes related to these groups as well monomer and dimers are observed in the same region.

4.5.1.3. Skeletal modes. The C═O, C═C, C═N, C—O, C—C and C—N stretching modes are expected in monomer and dimers of NPB. The C═O stretching modes are clearly predicted in all these derivatives, thus, in CPB this stretching mode is assigned at 1768 cm^{-1}, in MPB at 1759 cm^{-1} and in PB at 1763 cm^{-1}. In this derivative that mode is assigned to the strong IR band at 1770 cm^{-1}. Note that these C═O stretching modes follow the trend: NPB > CPB > MPB in accordance with the order observed in the dipole moment values: NO_2 > Cl > CH_3, being the CH_3 group activating while the Cl atom and NO_2 group act as deactivating. The C═N stretching modes are assigned in PB, CPB and MPB at 1692, 1624 and 1608 cm^{-1}, respectively. For NPB, the strong IR band at 1600 cm^{-1} is assigned to that vibration mode. In this case, these modes show not a defined

Table 3
Observed and calculated wavenumbers (cm^{-1}) and assignment for the 2-(4 nitrophenyl)-4H-3,1-benzoxacin-4-one.

Experimental[a]		B3LYP/6-31G*								
		Monomer			Dimer[b]					
IR solid	Ra solid				I		II		III	
		Cal	SQM	Assig[a]	Cal	Assig.	Calc	Assig.	Calc	Assig.
3192 vw	3194vw	3257	3122	νC21–H25	3259	ν C–H	3273	ν C–H	3258	ν C–H
3135vw	3138vw	3256	3121	νC19–H24	3257	ν C–H	3258	ν C–H	3256	ν C–H
	3111 vw	3242	3108	νC18–H22	3243	ν C–H	3255	ν C–H	3241	ν C–H
3107w		3238	3104	νC17–H20	3240	ν C–H	3238	ν C–H	3239	ν C–H
	3086w	3229	3096	νC5–H10	3233	ν C–H	3229	ν C–H	3239	ν C–H
3082w		3225	3092	νC2–H8	3225	ν C–H	3225	ν C–H	3226	ν C–H
	3075 w	3212	3079	νC6–H11	3217	ν C–H	3213	ν C–H	3217	ν C–H
	3063w	3197	3065	νC1–H7	3201	ν C–H	3198	ν C–H	3198	ν C–H
3053w	3052 sh			1571 + 1477						
3036sh	3035 vw			1770 + 1258						
3016vw	3010 vw			1520 + 4x372						
2930vw				3x688 + 869						
2872vw				1520 + 1359						
1770vs	1764w	1862	1792	νC9═O15	1860	νC═O	1840	νC═O	1843	νC═O
1742w					1859		1834		1840	
1626 s		1677	1621	νC21–C23	1677	νC═N	1676	νC═N	1678	νC═N
1626 s	1625s	1667	1612	νC1–C2	1665	νC═C	1666	νC═C	1666	νC═C
1626 s	1625s	1659	1603	νC18–C21	1658	νC═C	1657	νC═C	1659	νC═C
1600s	1598vs	1650	1594	νC12–N14	1649	νC═C	1650	νC═C	1649	νC═C
					1647					
1600s	1598vs	1620	1566	νC3–C4	1619	νC═C	1619	νC═C	1619	νC═C
1574w	1571s				1611	$\nu_a NO_2$	1612	$\nu_a NO_2$	1613	$\nu_a NO_2$
1520vs	1530vw	1613	1554	$\nu_a NO_2$	1539	βC–H	1536	βC–H	1539	βC–H
1495w	1494sh	1539	1492	βC19–H24	1517	βC–H	1518	βC–H	1520	βC–H
1477w	1477s	1518	1470	βC5–H10	1509	βC–H	1511	βC–H	1509	βC–H
1464w	1465w	1510	1465	βC6–H11	1451	βC–H	1450	βC–H	1452	βC–H
1413w	1413vw	1452	1408	νC17–C19						
1359s	1356s	1396	1348	$\nu_S NO_2$	1396	$\nu_S NO_2$	1397	$\nu_S NO_2$	1396	$\nu_S NO_2$
1359s	1356s	1381	1330	νC16–C18	1380	νC–C	1382	ν C–C	1381	ν C–C
		1371	1320	νC2–C3	1371		1373		1372	
1359s	1356s	1350	1313	βC2–H8	1350	βC–H	1352	βC–H	1353	βC–H
	1332vw	1333	1299	βC18–H22	1333	βC–H	1331	βC–H	1333	βC–H
1320m	1321w				1300	βC–H βR_1 (A2)	1299	νC–N	1300	νC–N
1258s	1258s				1297	νC–N	1298	νC–N	1297	νC–N
1258s	1258s	1300	1255	νC3–N14	1280	βC–H	1280	βC–H	1285	βC–H
1258s	1258s	1281	1242	νC4–C5	1244	βC–H βR_1(A3)	1247	βC–H	1246	βC–H
1225m		1243	1208	νC4–C9	1209	βC–H	1208	βC–H	1209	νC–C
1181sh	1179w	1209	1174	βC17–H20	1192	βC–H	1191	βC–H	1193	βC–H
1161vw	1161vw	1191	1157	βC1–H7	1139	βC–H	1140	βC–H	1145	βC–H
1110w	1113sh	1139	1109	νC5–C6	1139	βC–H	1139	βC–H	1138	βC–H
		1138	1105	βC21–H25	1131	νC–NO_2	1130	νC–NO_2	1131	βC–H
1067m	1078sh	1130	1096	νC19–C23	1097	βC–H	1091	βR_2(A3)	1096	βC–H
				νC23–N26				νC–O		νC–O
1067m	1066w	1097	1059	νC12–O13	1060	βC–H	1064	βC–H	1066	βC–H
1037w	1038w				1034	βC–H	1034	βC–H	1034	βR_1 (A3)
	1024sh	1060	1024	νC6–C1			1025	νC–O	1025	γC–H
									1017	
1012sh	1016vw	1034	1013	βR_1(A3)	1009	νC–O	1008	γC–H	1019	νC–O
					1007				1015	
1003m	1003vw	1009	998	γC17–H20	1005	γC–H	1001	γC–H	1007	γC–H
					1003					
1003m	998sh	1007	997	γC1–H7	1002	γC–H			996	γC–H
1003m		1006	986	γC18–H22	995	γC–H			992	γC–H
1003m		996	983	νC9–O13			980	γC–H		
975w	950vw	979	968	γC5–H10	978	γC–H	940	βR_1 (A2)	940	βR_1(A2)
925w	925vw	937	915	βR_1 (A2)	937	βR_2 (A2)	911	γC–H		
906vw		902	890	γC2–H8	902	γC–H	903	γC–H	912	γC–H
888vw	883sh	894	885	γC19–H24	893	γC–H	880	βR_2A1 βR_3A3	895	γC–H
869m	865vw	880	861	βR_1 (A1)	879	βR_2(A1,A3)	871	γC–H	879	βR_1 (A1)
865sh	847w	862	852	γC21–H25	860	γ(C–H)			863	γC–H
845w	842sh	857	844	δNO_2	857	δNO_2	858	δNO_2	857	δNO_2
819w		797	785	γ C6–H11	797	γC–H	798	γC–H	803	γC–H
792vw	787sh	792	774	τR_1 (A1)	790	γC–H	792	γC–H	794	γC–H
775s	777vw	774	760	γ NO_2	775	γ NO_2	775	γ NO_2	774	γ NO_2
761w	764vw	759	742	βR_2 (A3)	759	βR_3 (A1,A2)	762	βR_3 A1 βR_2 A2	761	βR_2(A1,A2)
749vw	748w	720	708	βR_2 (A1)	720	βR_3 (A3)	723	γC–H	721	βR_2 (A3)

Table 3 (*continued*)

Experimental[a]		B3LYP/6-31G*								
		Monomer			Dimer[b]					
IR solid	Ra solid				I		II		III	
		Cal	SQM	Assig[a]	Cal	Assig.	Calc	Assig.	Calc	Assig.
706w	708w	719	708	γ C16–C12	718	γ C–H	722	βR_3 (A3)	718	γC–H
706w	708w	696	681	γ C9=O15	695	γC=O	698	γC=O	699	γC=O
688m		680	661	τR_1 (A3)	679	τR_1 (A3)	682	τR_1 (A3)	680	τR_1 (A3)
670w	641sh	647	641	βR_3 (A3)	646	τR_2 (A3)	647	τR_2(A3)	647	βR_3(A3)
636w	635vw				633	βC=O	633	βC=O	633	βC=O
621vw	623vw	633	629	β(C9=O15)						
602vw	618sh				602	τR_1 (A1)	603	τR_1 (A1)	602	βR_3(A1)
591w	590vw	602	596	βR_3 (A1)						
564vw		550	541	βR_3 (A2)	550	τR_2(A1)	552	τR_1 A2	553	βR_3 (A2)
							551			
543vw	543vw	548	535	Butt(A1-A2)	548	Butt(A1-A2)			549	τR_1(A1)
532w	537sh	535	530	ρNO_2	536	ρNO_2	536	ρNO_2	535	ρNO_2
492vw		490	484	βR_2 (A2)	490	τR_1 A2	491	τR_2 A2	491	τR_2 A1
										τR_1 A2
475w	485w						482	τR_2 A3		
463sh	473sh	478	466	τR_3 (A3)	478	γC–N			477	τR_2 A3
454vw		449	438	νC23–NO_2	449	νC–NO_2	449	νC–NO_2	449	ν C–NO_2
441w		438	425	τR_2 (A1)	438	τR_3A1	438	τR_2 A1	442	τR_3 A1
428vw	429vw	420	407	τR_2 (A3)	422	τR_3 (A3)	422	τR_3 (A3)	420	τR_3(A3)
379m							377	β(A2–A3)		
372s	373vw	375	370	β(A2-A3)	374	β(A2-A3)			375	β(A2–A3)
	340vw	325			326	γC–N	326	τR_2(A2)	326	β(C–NO_2)
	317w		316	τR_3 (A1)						
	306vw				301	β(C=O)	305	β(C=O)	303	β(C=O)
	297vw	301	298	β(C9=O15)						
	245w	243	238	γC23–N26	246	τR_3 (A3)	245	Butt(A1-A2)	244	Butt(A1-A2)
	225vw	226	224	β(C23–NO_2)	226	β(C–NO_2)	229	β(C–NO_2)	228	β(C–NO_2)
	215sh	213	208	νC12–C16	213	νCA2–CA3	214	νCA2–CA3	213	νCA2–CA3
	193vw	156	152	τR_3(A2)	158	Butt(A1-A2)	158	τR_3 (A1)	158	Butt(A1-A2)
					157		157			
		136	133	τR_1(A2)	139	γC=O	142	γC=O	142	γC=O
		96	93	τR_2(A2)	98	γ C–C	97	γ C–C	97	τR_2 (A2)
		78	78	β(C12–O13)	79	τR_3 (A3)	83	β(C=C)	82	β(C=C)
		66	63	τwNO_2	75	τwNO_2	75	τwNO_2	66	τwNO_2
		39	38	γ C12–C16	38	τwNO_2	38	τwNO_2	34	τwNO_2
		33	32	τ(A2-A3)	37	τ(A2-A3)	28	τ(A2-A3)	24	τ(A2-A3)

Abbreviations: ν, stretching; β, deformation in the plane; γ, deformation out of plane; wag, wagging; τ, torsion; βR, deformation ring τ_R, torsion ring; ρ, rocking; τw, twisting; δ, deformation; Butt, butterfly; a, antisymmetric; s, symmetric; A1, Ring 1; A2, Ring 2.

[a] This work.

[b] DFT B3LYP/6-31G*.

Table 4
Comparison of scaled internal force constants for the 2 the 2-(4 nitrophenyl)-4H-3,1-benzoxacin-4-one).

B3LYP method						
Force constant	NPB		CPB		MPB	
	6-31G*	6-311++G**	6-31G*	6-311++G**	6-31G*	6-311++G**
f(νC=O)	12.758	12.462	12.685	12.385	12.629	12.305
f(νC–N)	7.590	7.473	7.575	7.458	7.556	7.434
f(νC–O)	4.644	4.460	4.639	4.450	4.640	4.455
f(νC12–C16)	4.884	4.794	4.948	4.858	4.964	4.873
f(νC23–X26)	3.999	3.763	3.304	3.256	4.375	4.306
$f(\nu C–C)_{ring}$	6.368	6.244	6.358	6.230	6.341	6.209
$f(\nu C–H)_{ring}$	5.266	5.180	5.235	5.155	5.200	5.124
f(νN=O)	9.735	9.392				

Units are mdyn $Å^{-1}$ for stretching and stretching/stretching interaction and mdyn Å rad^{-2} for angle deformations.
X26 = N, for NPB; Cl, for CPB; C, for MPB.

tendency (PB > CPB > MPB > NPB). For NPB, the C=C stretching modes are predicted in the expected regions expected for these derivatives [13,14], thus, the bands observed between 1626 and 1600 cm^{-1} are assigned to those stretching modes, as indicated in Table 3. The two C12–O13 and C9–O13 stretching modes that belong to the oxazin ring in the monomer are clearly assigned to the bands of the medium intensities at 1067 and 1003 cm^{-1}, respectively while these modes in the three dimers are predicted between 1097 and 1007 cm^{-1}. As observed in the MPB (243 cm^{-1}) and CPB (217 cm^{-1}) derivatives, the benzoxazin-nitrophenyl stretching inter-rings for NPB are predicted by SQM calculations at 208 cm^{-1}, thus, the introduction of a NO_2 group in the phenyl

ring linked to the benzoxazin ring generate a shifting toward lower wavenumbers. The C–C and C–N stretching modes and those rings deformations and torsions related to the three A1, A2 and A3 rings were performed taking into account the assignments reported for the derivatives CPB and MPB [13,14].

4.6. Force field

The force constants for NPB were calculated by using the B3LYP/6-31G* and B3LYP/6-311++G** methods with the Molvib program [24], as explained in section computational details. The results are summarized in Table 4 together with those reported for CPB and MPB [13,14]. Note that the *f(νC=O)* force constants with both basis sets follow the trend: NPB > CPB > MPB in agreement with the assignations performed for the C=O stretching modes. A similar relation was also observed in the *f(νC–N)* force constants with both basis sets. Here, an interesting result is observed when the *f(νC12–C16)* force constants related to the benzoxazin-nitrophenyl stretching inter-rings values are compared because the values increase from NPB > CPB > MPB in disagree with the tendency observed in their corresponding wavenumbers. Hence, obviously these results cannot be explained from that point of view but, they can be justified analyzing the HOMO values because the reactivity increase according the following order: NPB > CPB > MPB, which explains the higher reactivity for MPB due to the activating group that makes most reactive the benzoxazin-4-one ring. In this study, it is very important to analyze the *f(νC23-X26)* force constants which follow the tendency: MPB > NPB > CPB. This trend can be clearly explained by the stabilities orders because with both basis sets that properties increase according to the tendency: CPB > NPB > MPB.

5. Conclusions

In this work, the 2-(4-nitrophenyl)-4H-3,1-benzoxazin-4-one derivative was experimentally characterized by FTIR and FT-Raman spectroscopies in the solid phase while the molecular structures of the monomer and three dimeric species of that derivative were theoretically determined at the B3LYP/6-31G* and B3LYP/6-311++G** levels of theory. Here, the structural and vibrational properties were predicted and compared with those reported for the chlorinated (Cl-PB) and methylated (NO_2-PB) derivatives at the same levels of theory. The observed variations in the properties are clearly justified by the activating (CH_3) and deactivating (NO_2 and Cl) characteristics of the different groups. Thus, both C12–N14 and C12–Cl14 bonds in the corresponding derivatives show double bond characters as a consequence of their deactivating features while those two deactivating substituent make less reactive the benzoxazin-4-one ring stabilizing the compound, as observed by NBO and AIM analyses. Hence, the following stability orders: Cl-PB > NO_2-PB > CH_3-PB can be clearly observed. The frontier orbitals studies reveal that the Cl-PB and NO_2-PB derivatives have good stabilities and high chemical hardness while CH_3-PB has a higher chemical reactivity. Thus, these results are in very good agreement with those similar found by NBO and AIM studies. On the other hand, the presence of the IR bands at 1574 and 1037 cm^{-1} and, of the Raman bands at 1571 and 1038 cm^{-1} support clearly the presence of the different dimeric species proposed for NPB. Here, the force fields and the complete vibrational assignments are also reported for NPB together with the corresponding force constants. Finally, the trend observed in the *f(νC23-X26)* force constants support the observed stabilities orders: Cl-PB > NO_2-PB > CH_3-PB.

Acknowledgements

This work was supported with grants from CIUNT Project N° 26/D507 (Consejo de Investigaciones, Universidad Nacional de Tucumán). The authors thank Prof. Tom Sundius for his permission to use MOLVIB.

Appendix A. Supplementary data

Supplementary data related to this article can be found at http://dx.doi.org/10.1016/j.molstruc.2016.08.070.

References

[1] D. Romani, M.J. Márquez, M.B. Márquez, S.A. Brandán, Structural, topological and vibrational properties of an isothiazole derivatives series with antiviral activities, J. Mol. Struct. 1100 (2015) 279–289.
[2] D. Romani, S.A. Brandán, Structural, electronic and vibrational studies of two 1,3-benzothiazole tautomers with potential antimicrobial activity in aqueous and organic solvents, Predict. Their React. Comput. Theor. Chem. (Theochem) 1061 (2015) 89–99.
[3] E. Romano, M.V. Castillo, J.L. Pergomet, J. Zinczuk, S.A. Brandán, Synthesis, structural and vibrational analysis of (5,7-Dichloro-quinolin-8-yloxy) acetic acid, J. Mol. Struct. 1018 (2012) 149–155.
[4] M.V. Castillo, E. Romano, A.B. Raschi, A. Yurquina, S.A. Brandán, Structural study and vibrational spectra of 3-amino -2-(4-chlorophenyl) quinazolin-4(3H)-one, Comp. Theor. Chem. 995 (2012) 43–48.
[5] E. Romano, J.L. Pergomet, J. Zinczuk, S.A. Brandán, Structural and Vibrational Properties of Some Quinoline Acetic Acid Derivatives with Potentials Biological Activities. Acetic Acids: Chemical Properties, Production and Applications, Edited Collection, Nova Science Publishers, Inc, 2013. Angelo Basile (Technology of the National Research Council, Rende, Italy), (Chapter 3), ISBN: 978-1-62948-217-0.
[6] D. Lednicer, The Organic Chemistry of Drug Synthesis, vol. 7, Wiley-Interscience. A John Wiley & Sons, Inc., Hoboken, New Jersey, 2008.
[7] K. Waisser, L. Kubicova, V. Buchta, P. Kubanova, K. Bajerova, L. Jiraskova, Folia Microbiol. 47 (2002) 488.
[8] V.K. Pandey, S. Yadava, K. Chandra, M.N. Joshi, S.K. Bajpai, Indian Drugs 36 (1999) 532.
[9] C. Altinkok, B. Kiskan, Y. Yagci, Synthesis and characterization of sulfone containing main chain oligobenzoxazine precursors, J. Polym. Sci. Part A Polym. Chem. 49 (2011) 2445–2450.
[10] M.A. El-Hashash, S.A. Rizk, Synthesis and utility of 6-(β-phthalimidoethyl)-2-methyl and/or 2-phenyl-3,1-benzoxazin-4-ones in some heterocyclic synthesis, Middle-East J. Sci. Res. 11 (4) (2012) 541–549.
[11] S. Venkataraman, R. Meera, Pandiarajan P. Devi, Synthesis and biological activity of some novel quinazolinone derivatives, J. Chem. Pharm. Res. 2 (5) (2010) 461–475.
[12] L. Rai, Synthesis of Quinazoline Analogues of Biological Interest, Al-Ameen Collegue of Pharmacy, Hosur Road, Bangalore, India, 2010. Master of Pharmacy in Pharmaceutical Chemistry.
[13] María V. Castillo, Elida Romano, Gerardo R. Argañaraz, Roxana A. Rudyk, Silvia A. Brandán, Chapter 1, Theoretical Structural and Vibrational Investigation on the 2-(4-chlorophenyl) -4H-3,1-benzoxazin-4-one Compound. Structural Analysis and Modelling: Research and Development, Edited Collection, Nova Science Publishers, Inc., 2013. ISBN: 978-1-62618-674-3.
[14] M.V. Castillo, E. Romano, A.B. Raschi, S.A. Brandán, Chapter 12, Structural and Vibrational Investigation on a Benzoxazin Derivative with Potential Antibacterial Activity, Frontiers in Computational Chemistry, Editorial Bentham Science Publishers, 2014.
[15] A.B. Nielsen, A.J. Holder, *Gauss View* 3.0, User's Reference, GAUSSIAN Inc., Pittsburgh, PA, 2000–2003.
[16] A.D. Becke, Density functional thermochemistry. III. The role of exact exchange, J. Chem. Phys. 98 (1993) 5648–5652.
[17] C. Lee, W. Yang, R.G. Parr, Development of the Colle-Salvetti correlation-energy formula into a functional of the electron density, Phys. Rev. B 37 (1988) 785–789.
[18] M.J. Frisch, G.W. Trucks, H.B. Schlegel, G.E. Scuseria, M.A. Robb, J.R. Cheeseman, J.A. Montgomery Jr., T. Vreven, K.N. Kudin, J.C. Burant, J.M. Millam, S.S. Iyengar, J. Tomasi, V. Barone, B. Mennucci, M. Cossi, G. Scalmani, N. Rega, G.A. Petersson, H. Nakatsuji, M. Hada, M. Ehara, K. Toyota, R. Fukuda, J. Hasegawa, M. Ishida, T. Nakajima, Y. Honda, O. Kitao, H. Nakai, M. Klene, X. Li, J.E. Knox, H.P. Hratchian, J.B. Cross, C. Adamo, J. Jaramillo, R. Gomperts, R.E. Stratmann, O. Yazyev, A.J. Austin, R. Cammi, C. Pomelli, J.W. Ochterski, P.Y. Ayala, K. Morokuma, G.A. Voth, P. Salvador, J.J. Dannenberg, V.G. Zakrzewski, S. Dapprich, A.D. Daniels, M.C. Strain, O. Farkas, D.K. Malick, A.D. Rabuck, K. Raghavachari, J.B. Foresman, J.V. Ortiz, Q. Cui, A.G. Baboul, S. Clifford, J. Cioslowski, B.B. Stefanov, G. Liu, A. Liashenko, P. Piskorz, I. Komaromi, R.L. Martin, D.J. Fox, T. Keith, M.A. Al-Laham, C.Y. Peng, A. Nanayakkara, M. Challacombe, P.M.W. Gill, B. Johnson, W. Chen,

M.W. Wong, C. Gonzalez, J.A. Pople, Gaussian 03, Revision B.01, Gaussian, Inc., Pittsburgh PA, 2003.
[19] A.E. Reed, L.A. Curtis, F. Weinhold, Intermolecular interactions from a natural bond orbital, donor-acceptor viewpoint, Chem. Rev. 88 (6) (1988) 899–926.
[20] E.D. Glendening, J.K. Badenhoop, A.D. Reed, J.E. Carpenter, F. Weinhold, NBO 3.1, Theoretical Chemistry Institute, University of Wisconsin, Madison, WI, 1996.
[21] B.H. Besler, K.M. Merz Jr., P.A. Kollman, Atomic charges derived from semi-empirical methods, J. Comp. Chem. 11 (1990) 431–439.
[22] F. Biegler-Köning, J. Schönbohm, D. Bayles, AIM2000; a program to analyze and visualize atoms in molecules, J. Comput. Chem. 22 (2001) 545.
[23] R.F.W. Bader, Atoms in Molecules, a Quantum Theory, Oxford University Press, Oxford, 1990. ISBN: 0198558651.
[24] T. Sundius, Scaling of Ab-initio force fields by MOLVIB, Vib. Spectrosc. 29 (2002) 89–95.
[25] a) G. Rauhut, P. Pulay, Transferable scaling factors for density functional derived vibrational force fields, J. Phys. Chem. 99 (1995) 3093–3099;
b) G. Rauhut, P. Pulay, J. Phys. Chem. 99 (1995) 14572.
[26] R.G. Parr, R.G. Pearson, J. Am. Chem. Soc. 105 (1983) 7512–7516.
[27] R. Thilagavathy, H.P. Kavitha, R. Arulmozhi, J.P. Vennila, V. Manivannan, 2-Phenyl-4*H*-3,1-benzoxazin-4-one, Acta Cryst. E65 (2009) o127.
[28] E.R.T. Tiekink, J.L. Wardell, 2-(2-Amino-4-nitro-phen-yl)-7-nitro-4*H*-3,1-benzoxazin-4-one, Acta Cryst. E70 (2014) o158–o159.
[29] J.-L. Brédas, Mater. Horiz. 1 (2014) 17–19.
[30] M.J. Márquez, M.B. Márquez, P.G. Cataldo, S.A. Brandán, Open J. Synth. Theory Appl. 4 (2015) 1–19.
[31] P.G. Cataldo, M.V. Castillo, S.A. Brandán, J. Phys. Chem. Biophys. 4 (1) (2014) 2–9. M.B. Márquez, S.A. Brandán, International J. of Quantum Chem. 114(3) (2014) 209–221.
[32] D. Romani, S.A. Brandán, Structural and spectroscopic studies of two 1,3-benzothiazole tautomers with potential antimicrobial activity in different media, Predict. Their React. Comput. Theor. Chem. 1061 (2015) 89–99.
[33] D. Romani, M.J. Márquez, M.B. Márquez, S.A. Brandán, Structural, topological and vibrational properties of an isothiazole derivatives series with antiviral activities, J. Mol. Struct. 1100 (2015) 279–289.